



Observations and modeling of tsunami-induced currents in ports and harbors

Patrick J. Lynett ^{a,*}, Jose C. Borrero ^{a,b}, Robert Weiss ^c, Sangyoung Son ^a,
Dougal Greer ^b, Willington Renteria ^d

^a Department of Civil and Environmental Engineering, University of Southern California, Los Angeles, CA 90089 USA

^b ASR Limited, Marine Consulting and Research, Raglan, 2531 New Zealand

^c Department of Geosciences, Virginia Tech, Blacksburg, VA 24061 USA

^d Department of Civil Engineering, Texas A&M University, College Station, TX 77843 USA

ARTICLE INFO

Article history:

Received 7 September 2011

Received in revised form 31 January 2012

Accepted 4 February 2012

Available online xxx

Editor: P. Shearer

Keywords:

tsunami
whirlpools
eddies
turbulent structures
field observation
numerical simulation

ABSTRACT

Tsunamis, or “harbor waves” in Japanese, are so-named due to common observations of enhanced wave heights, currents and damage in harbors and ports. However, dynamic currents induced by these waves, while regularly observed and known to cause significant damage, are poorly understood. Observations and modeling of the currents induced by the 2011 Tohoku and 2004 Indian Ocean tsunamis allows us to show that the strongest flows in harbor basins are governed by horizontally sheared and rotational shallow features, such as jets and large eddies. When examining currents in harbors, this conclusion will generally require a simulation approach that both includes the relevant physical processes in the governing equations and uses a numerical scheme that does not artificially damp these features. Without proper representation of the physics associated with these phenomena, predictive models may provide drag force estimates that are an order of magnitude or more in error. The immediate implementation of this type of analysis into tsunami hazard studies can mean the difference between an unaffected port and one in which 300 m long container vessels are detached from their moorings and drift chaotically.

© 2012 Elsevier B.V. All rights reserved.

1. Introduction and background

Basin resonance and geometric amplification are two reasonably well understood mechanisms for local magnification of tsunami impact in harbors (Raichlen, 1966; Synolakis, 2004), and are generally the mechanisms investigated when estimating the tsunami hazard potential in a port or harbor (Borrero et al., 2005). On the other hand, our understanding of and predictive ability for currents is lacking. Many records of tsunami effects note large shallow coherent turbulent structures, more commonly referred to as whirlpools. Observations of tsunami-induced whirlpools have been described throughout history; glyphs and carvings of indigenous peoples in the Pacific Northwest depict tsunami whirlpools associated with sea monsters, making the ocean boil and swallowing fisherman (Ludwin and Colorado, 2006). We remark here that while these large turbulent eddies are often referred to as whirlpools in the media and during casual discussions, the term whirlpool is most commonly connected to a horizontal vortex with a strong downdraft in the center (i.e. the drain analogy). The physics of the structures examined here are quite different, and thus the descriptor whirlpool will not be employed for the rest of the paper.

More recent history is detailed with accounts from ship captains and harbor masters. An 1867 earthquake in the Lesser Antilles caused extreme damage in many Caribbean ports (Reid and Taber, 1920). In the Port of Saint Thomas, an Admiral of the U.S. Navy noted the formation of a large eddy in the center of the bay, pulling floating debris towards it. Another Naval vessel in the port was spun around 20 times in the receding waves, until finally settling in the large gyre in the center of bay, spinning slowly for hours. During the 2004 Indian Ocean tsunami, damage to harbors was noted in a series of papers by Okal et al. (2006a,b,c). The most remarkable of these events occurred in the Port of Salalah, Oman. About 90 min after tsunami first arrival, strong currents near the most offshore unloading berth broke all of the mooring lines on a 285-m ship and pulled it away from the terminal. The vessel then drifted on the currents for hours, spinning numerous times, before beaching on a nearby sandbar.

Here we put forth that, during tsunami events, the damaging currents inside ports and harbors are driven by coastal-structure-induced or topographically-controlled fluid jets and large shallow turbulent coherent structures. Furthermore, when there is little or no flooding of port facilities, as would typically be the case unless the incoming tsunami was extremely large, the only significant mechanism for damage is the currents. A clear example of this is the previously discussed Salalah Port during the 2004 tsunami; here the maximum tsunami elevation was a relatively small 1.5 m (Okal et al., 2006a), yet the currents were strong enough to break all 12 of

* Corresponding author.

E-mail address: plynnett@usc.edu (P.J. Lynett).

the ~500 kN strength mooring lines on a large freighter (Gaythwaite, 2004). If the conclusion of this observation was that, in general, a “common” tsunami of approximately 1 m was capable of detaching the largest of ships in any given port, the required preparation and mitigation measures would likely be unmanageable and unreasonable. Here we will show, through a combination of observations and data from the 2011 Tohoku tsunami and complimentary modeling, that the strongest currents in a port are governed by horizontally sheared and rotational flow, and that the location of these features, while chaotic in the turbulent sense, can be reasonably predicted with an appropriate model. With an improved physical understanding of the creation and evolution of these complex features, ports and harbors should be better capable of identifying particularly vulnerable areas.

2. Observations: tsunami currents in ports during the Tohoku tsunami

The Tohoku tsunami provided one of the most comprehensive observational and instrumental data sets describing both near and far-field tsunami effects on modern port infrastructure. While water surface elevation measurements are widespread, this is not the case for water current measurements. In this section, we describe select records of the limited set of tsunami current data and effects at sites in Japan, California, New Zealand and the Galapagos Islands.

In the extreme near field, the Port of Oarai in Japan provided the one of the most vivid examples of rotational currents (BBC, 2011, and other widespread news coverage). A snapshot of the aerial video taken from a helicopter is shown in Fig. 1. This turbulent structure was filmed approximately 3 h after the earthquake, and thus well after the initial waves. Video of this eddy indicates its existence for tens of minutes, before it was likely flushed out by a following series of waves. The whitewater streaks seen throughout the rotating fluid are indicative of a complex 3D flow pattern with distinct areas of surface flow convergence and divergence.

In California, the most severe tsunami effects occurred in Crescent City (Wilson et al., 2011). Crescent City is well known for its tendency to amplify far-field tsunami surges (Horrillo et al., 2007; Kowalik et al., 2008) and experienced significant damage in 1964 following the great Alaska earthquake (Griffin, 1984) and more recently in 2006

by a tsunami generated in the Kuril Islands (Dengler et al., 2008). Repairs from that event were nearly complete when the harbor was yet again severely damaged by the Tohoku tsunami. Current speed time histories at the entrance to Crescent City’s inner harbor reconstructed from security camera footage indicated speeds of up to 8 knots (4 m/s), generally slower than estimates reported by experienced mariners who witnessed the event (Dengler et al., 2011). A current meter installed in Humboldt Bay, a natural bay and coastal lagoon located roughly 100 km south of Crescent City, recorded a detailed time history of the event. Maximum current speeds of 1.7 knots (0.9 m/s) were recorded and accurately simulated to first order using NOAA’s tsunami forecast model (Dengler et al., 2011). At Pillar Point harbor, south of San Francisco, the orientation of the harbor entrance and breakwaters induced a clockwise rotating vortex in the outer harbor basin with a smaller, counter clockwise rotation in the inner harbor (see Fig. 1). Local captains estimated the currents to be on the order of 5 to 10 knots (2.6–5.1 m/s). Indeed, significant and at times damaging currents were noted along the entire US West coast and were the main ‘story’ of this tsunami event.

Across the Pacific in New Zealand, several locations experienced strong and dangerous currents that primarily affected recreational maritime activities. At the Port of Tauranga in the Bay of Plenty, three water level gages and a current meter recorded the tsunami (Fig. 2). Water levels fluctuated on the order of ± 0.5 m while maximum current speeds (tsunami + tide) exceeded 4.5 knots (2.3 m/s), coinciding with the falling tide approximately 10 h after the tsunami first arrival. The maximum tsunami current (tidal component removed) was on the order of 2 knots and occurred shortly ~3 h after first arrival on the incoming tide. Looking at the tsunami perturbations in both the speed and water level, it is clear that relative to the “background” tidal speed and water level, the current deviations are significant. Spectral analysis of the tsunami signal indicates that the strongest currents occurred during peak tsunami energy which persisted for ~8 h after first arrival. It should be noted that these currents, although significant, did not disrupt operations at the Port of Tauranga.

In the Galapagos Islands, strong currents were noted in all of the main harbors including Puerto Ayora, where a tidal gage and a current meter recorded the event (Fig. 3). However, the 20 minute sample rate only provides a coarse representation of the current time histories. Note that the current meter is located in approximately 8 m water



Fig. 1. Selected sites where significant tsunami currents were observed during the Tohoku tsunami. (Left) Port of Oarai and the shallow turbulent coherent structure; (top right) tsunami surge jetting in to Crescent City’s inner harbor; (bottom right) Pillar Point Harbor which experienced counter rotating eddies in the inner and outer basins.

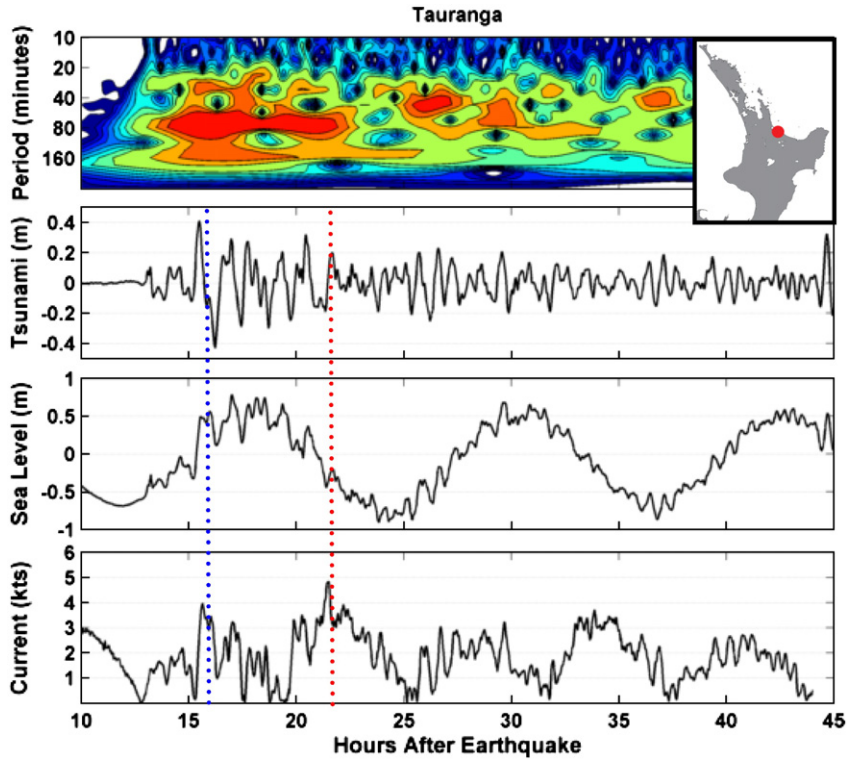


Fig. 2. Measured current speed, water level and spectral content from the Tohoku tsunami at Tauranga Harbour, New Zealand. The highest total current speed (tsunami + tide, red dashed line) occurred ~10 h after first arrival and corresponded with the falling tide. The highest tsunami-only current speed (tidal component removed, blue dashed line) occurred ~3 h after first arrival during the third and largest surge, mid way through the rising tide. The peak tsunami energy persisted for ~8 h after first arrival. (For interpretation of the references to color in this figure legend, the reader is referred to the web version of this article.)

depth, while the water level measurement is essentially at the shoreline in 2 m depth. Tsunami currents persisted for more than 24 h after the initial wave arrival. The maximum tsunami-induced currents, which are associated with the first waves, are ~0.6 knots (0.3 m/s). Note again, however, that the measurement location of this device is away from any structures or flow constrictions and in deeper water; the measured currents are very likely associated with straight-line currents of the water inflow and outflow.

3. Simulation: tsunami-induced hydrodynamics in ports

That strong currents are formed as tsunamis enter ports and harbors is not surprising to those that study such events (e.g. Okal et al., 2002). Likewise, when a free surface flow is forced through a geometric constriction, it is readily expected that the enhanced potential gradient will drive strong, possibly unstable currents with associated turbulent structures such as shallow coherent structures (Socolofsky and Jirka, 2004); a simple example would be tidal flow through an inlet channel. However, these fundamentals have not been quantitatively connected with respect to understanding tsunami hazards in ports and harbors. A plausible explanation for this oversight is the observation these eddies are turbulent phenomena with spatial and temporal scales much smaller than that of a typical tsunami. Our ability to model and then dissect them has only recently developed.

Ideally, one would use a fully three dimensional, turbulence-resolving hydrodynamic model to simulate the generation and evolution of jets and coherent structures near coastal infrastructure (e.g. Hinterberger et al., 2007). However, due to the spatial scale of these facilities (e.g. the Los Angeles/Long Beach Port complex encompasses more than 50 km²) and the need to properly couple the entire tsunami time history within a single simulation (Synolakis, 1995), researchers utilize simplifications and approximations. The approach presented here differs significantly from established tsunami hydrodynamic

simulations in that we use a multi-physics nested model, wherein a high-order Boussinesq-type model is embedded within a large-scale nonlinear shallow water solver. Specifically, this model, in addition to the standard Boussinesq terms, accurately accounts for horizontal and vertical turbulent mixing, bottom stress and depth averaging effects that might locally govern tsunami currents.

The governing equations utilized in the simulations to be presented here are given in dimensional form as:

$$\frac{\partial \eta}{\partial t} + \nabla \cdot [H\bar{u}] + E_{DISP} + E_{VISC} = 0 \quad (1)$$

$$\frac{\partial \bar{u}}{\partial t} + \bar{u} \cdot \nabla \bar{u} + g \nabla \eta + \bar{F}_{DISP} + \bar{F}_{VISC} + \bar{M}_{HOR} + \bar{M}_{VERT} + \frac{\tau}{\rho H} = 0 \quad (2)$$

where the continuity Eq. (1) is integrated in time to yield the ocean surface elevation, η , and the momentum Eq. (2) is integrated for \bar{u} , some reference horizontal velocity vector. Additionally, H is the water depth, g is gravity, ∇ is the horizontal gradient operator, t is time, τ is the bottom stress, ρ is the fluid density, and bold variables indicate horizontal vector quantities. Note that there is no vertical dependency in these models, as they are depth-integrated and fundamentally limited to hydrodynamic phenomena that have horizontal length scales much greater than the local water depth. This aspect also has implications for turbulence modeling. The vertical structure of the model is analytical; any turbulent 3D processes and their associated mixing must be handled in an averaged and approximate manner.

In the continuity equation, the two “E” terms represent 2nd-order corrections to the basic shallow water model, and provide frequency dispersion corrections (“DISP” subscript) and viscous corrections (“VISC” subscript). If the reference velocity, \bar{u} , is specified as the depth-averaged velocity, then these two “E” terms must by definition

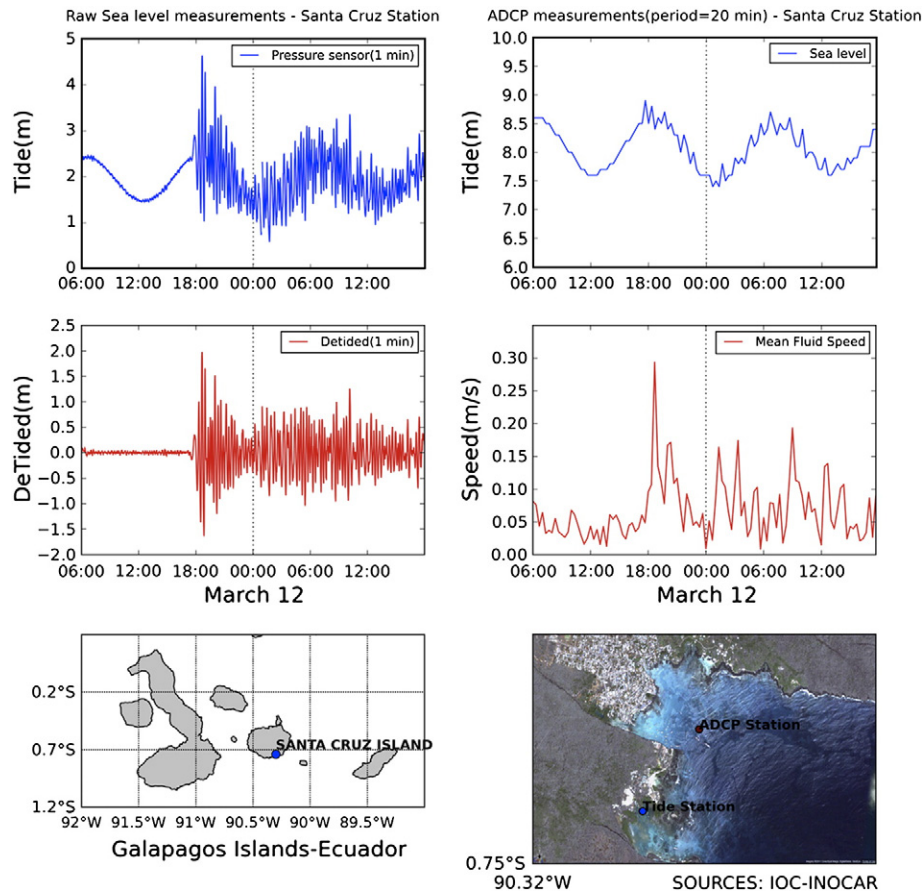


Fig. 3. ADCP current and sea surface elevation measured in Port Ayora during the tsunami event. (Upper left) Raw tidal data and de-tided signal for ocean surface elevation for data from tidal station (depth = 2 m); (Upper right) raw tidal water surface elevation data and fluid speed at the ADCP location (depth = 8 m); (Bottom left): overview of the Galapagos Islands and the location of Puerto Ayora; (Bottom right): GoogleEarth image of Puerto Ayora, showing both the ADCP and tide gage locations.

be zero; in many Boussinesq-type wave models, a velocity at an arbitrary elevation in the water column is used, and these terms are not zero. In the momentum Eq. (2), we similarly have the 2nd order correction “ \bar{F} ” terms as well as the “ \bar{M} ” mixing terms for both horizontal (“HOR” subscript) and vertical (“VERT” subscript) mixing. These mixing terms represent the turbulence closure scheme. Details of the turbulence closure used in this paper can be found in Kim and Lynett (2011) and is very similar to what is often used in shallow ocean circulation models, investigating for example nearshore tidal flow (e.g. Brière et al., 2007). Lastly, the bottom stress term is closed with some empirical relation, such as Moody’s or Manning’s equation. In traditional tsunami simulation, none of the “E”, “ \bar{F} ”, or “ \bar{M} ” terms are included, despite the demonstration that they all exist at the same order as the bottom stress term (Kim et al., 2009). These terms can become locally important in rotational and horizontally sheared flows, as indicated in Kim and Lynett (2011) and Son et al. (2011).

While the 2nd-order-corrected (high-order Boussinesq) model provides a more accurate representation of the relevant physics in shallow, turbulent flows, this accuracy comes at a significant computational cost. The number of operations hidden in the “E” and “ \bar{F} ” groupings is very large. Also, there exist third order spatial derivatives in these operations, thus requiring a fourth-order accurate numerical scheme for consistency. The computational cost of the high-order model is one to two orders of magnitude larger than the simpler, non-linear shallow water model used in typical tsunami studies, given the same grid and time step properties. In the following section, we will present simulation results from this high-order, Boussinesq-type approach and compare with predictions from an established shallow water model. In these simulations, the horizontal grid length used is

5 m and the seafloor roughness is approximated with a Manning’s roughness coefficient of $n=0.02$, a value characteristic of a smooth and even ocean bottom.

4. Results and discussion: tsunami-induced jet and eddy properties

We developed hydrodynamic models for tsunami induced currents from the Tohoku tsunami at Oarai Port in Japan and Pillar Point Harbor in California. The models use the USGS (2011) finite fault model as the hydrodynamic initial condition with bathymetry derived from online NOAA National Geophysical Data Center data sources and nautical charts. The model COMCOT (Wang and Liu, 2006) is used to propagate the tsunami signal from the source to each location, where detailed simulations on fine scale bathymetry are carried out using the higher order Boussinesq techniques described above.

Fig. 4 provides a simulation snapshot of the mid-depth vertical vorticity in the Port of Oarai at approximately the same time as the aerial views of the giant eddy shown in Fig. 1. Vorticity, a measure of a fluids circulation or rotation, is calculated as the curl of the 3D velocity field. For our purposes, we focus on rotation in the horizontal plane, given as $\partial v / \partial x - \partial u / \partial y$, where “v” is the velocity component in the y-direction and “u” the component in the x-direction. In the simulation, both the reach of the overall circulation and the diameter of the inner vortex core are qualitatively reproduced. The inner core is wrapped in an outer ring of very high flow speeds, predicted to be in excess of 6 m/s (11.6 knots). Typical of a shallow coherent structure, the horizontal velocities vanish near the center, where weak upwelling is predicted and expected (Jirka, 2001). This last point is particularly relevant as during the event, some news correspondents, in an attempt to describe the phenomena to a general audience, invoked the drain (or toilet bowl)

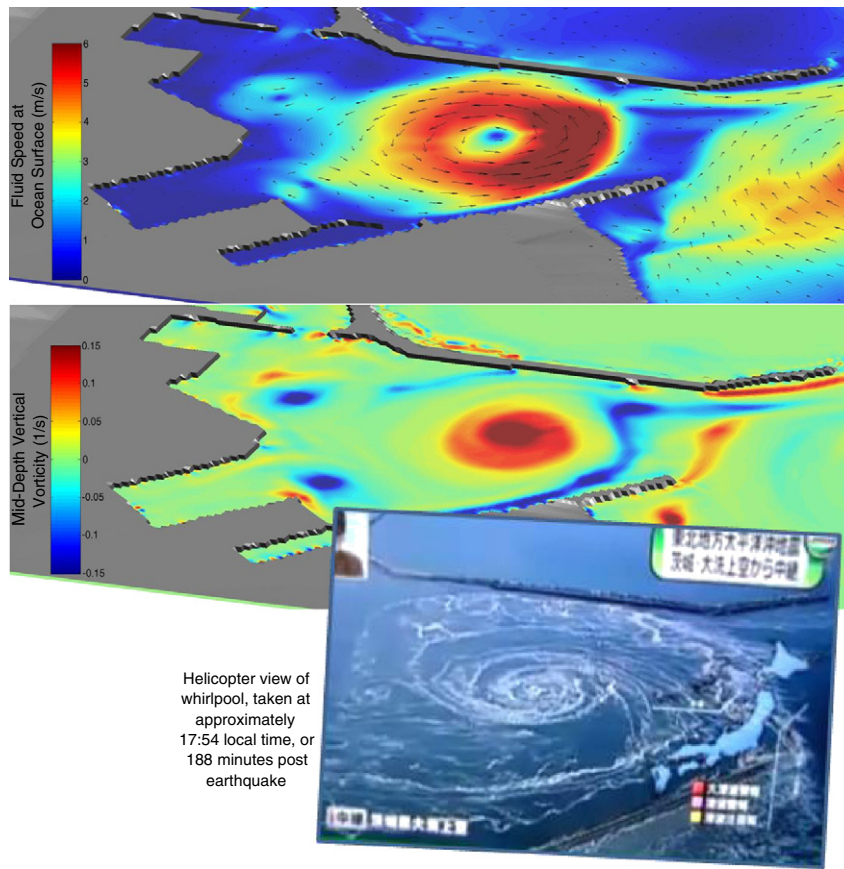


Fig. 4. Numerical model results of the Tohoku tsunami in the Port of Oarai. Snapshots are from 188 min after the earthquake. (top) Fluid speed, (middle) vertical vorticity at mid-depth, and (bottom) aerial image of the rotational feature at approximately the same time.

analogy, stating that objects would be sucked underwater when reaching the center.

In the Pillar Point simulation, both the incident tsunami amplitude and the current magnitude are significantly smaller than at near field locations such as Oarai. Fig. 5 provides an observation and the numerical recreation of currents inside the harbor. In the photograph, taken

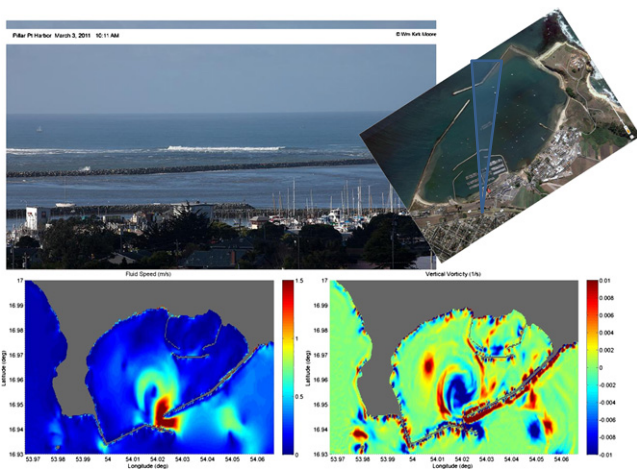


Fig. 5. Numerical model results of the Tohoku tsunami in Pillar Point Harbor, CA. All images are from 12 h and 26 min after the earthquake (10:11 am local time). (top left): Photograph of the coherent structure inside of the outer breakwaters; (top right) a Google Earth image of the Harbor showing the field of view of the photograph; (bottom left) fluid speed; (bottom right): vertical vorticity.

12.4 h after the earthquake, the curved ocean surface streaking indicative of rotational current is evident. This coherent structure has a diameter of roughly 50 m, and has been recently created by the jet-like inflow of a flooding wave. Two snapshots from the numerical simulation show the fluid speed and the vertical vorticity at the same time. The signature of rotation is clear in both, with flow speeds of 0.75–1.0 m/s in the vortex ring; such a predicted speed is reasonably consistent with the smooth ocean surface recorded in the photograph. The simulation predicts maximum flood speeds of 3–6 m/s (6–12 knots) in and immediately around the breakwater gap, which is in-line with the qualitative estimates from eyewitnesses.

Finally, the model is applied to hindcast and quantifies the effect of sheared and rotational flows observed at the Port of Salalah, Oman during the 2004 Indian Ocean tsunami. Fig. 6 shows the maximum fluid speed recorded over the entire tsunami event for a simulation with resolved rotational features and for a simulation without these features. The rotational model is the high-order Boussinesq model discussed and used above, while the other results are from a shallow water equation model wherein the relatively small vortices are damped out through numerical dissipation. The shallow water model is COMCOT, which due to the upwind differencing employed in the model, has significant numerical dissipation when the flow curvature is large (see Son et al., 2011 for additional details); shallow water models without low-order numerical dissipation would yield results different from those presented here from COMCOT. While the fluid speed predictions are quite different between the models, the predicted water surface elevations at the tidal station inside the port are very similar and in good agreement with the measured data. Near the initial location of the ship pulled from its moorings, the eddy resolving model predicts a flow speed near 6 m/s (~11 knots) with high horizontal shear, while the non-resolving COMCOT model predicts

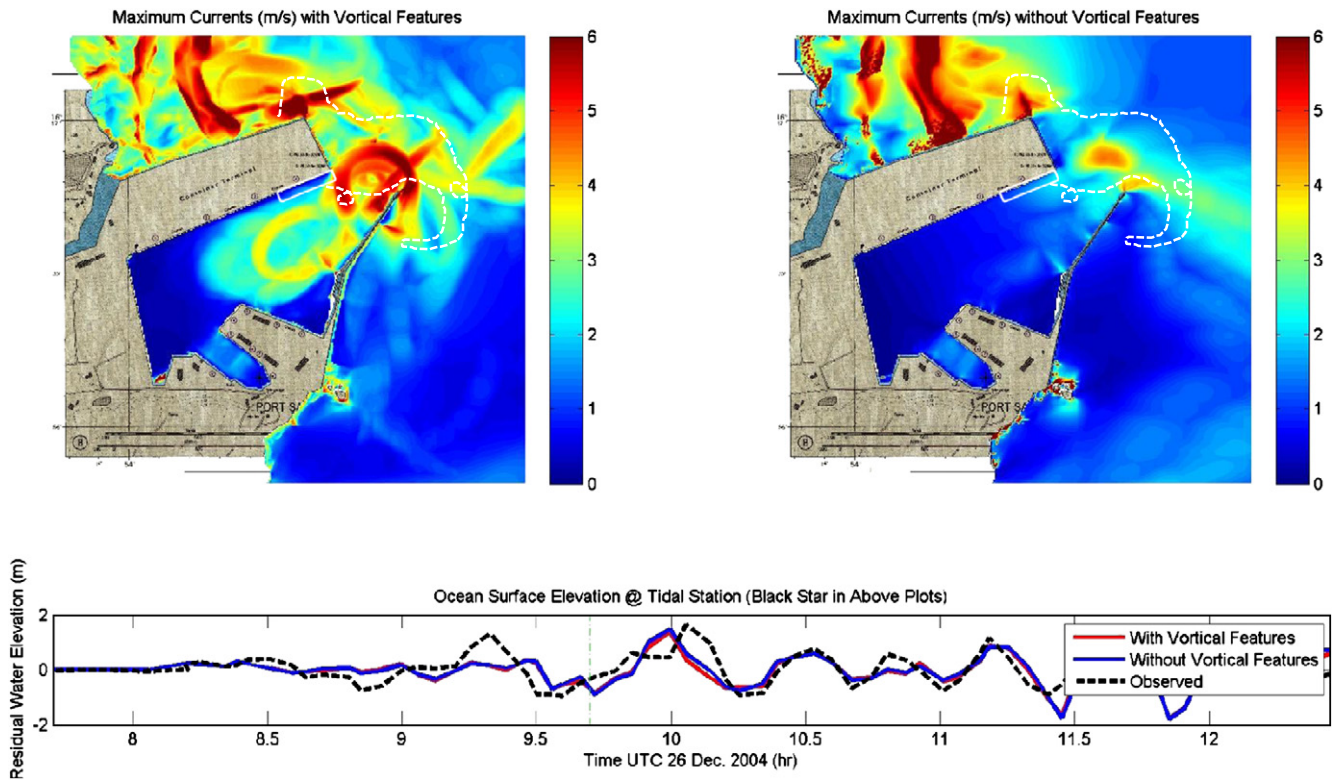


Fig. 6. Numerical model results of the 2004 Indian Ocean tsunami in Salalah, Oman. (top left) Maximum current speed using the higher-order eddy resolving model and (top right) a model that damps out the eddies. (bottom) Modeled water surface elevation time histories inside the Port; green vertical line indicates the time that the vessel broke its mooring lines. The initial location of the vessel is shown by the white rectangle, and the path of the ship after detachment is given by the dashed white line. Path is approximate and digitized from un-scaled hand drawings presented in Okal et al. (2006b).

locally-uniform speeds less than 2 m/s (~ 3.8 knots). As drag force is proportional to velocity squared, this factor-of-three difference in the predicted maximum current speed roughly equates to a nine-fold difference in the drag force; the eddy-resolving model predicts possible fluid drag forces that are nine times greater than the predictions of COMCOT. If the vessel rotates, even slightly, with the sheared flow, mooring lines will not equally transfer the increasing drag force on the vessel to the tie-down anchor, leading to a situation where the mooring lines break sequentially as the vessel is rotated away from its berth. The maximum currents in this area are associated with a wave flooding the port between 9:30 and 10:00 UTC; the ship broke its moorings at 9:42 UTC.

5. Conclusions

The Salalah modeling example (Fig. 6) shows that the accurate prediction of water surface elevations (the present goal of most tsunami hazard mitigation studies) does not necessarily correlate with an accurate prediction of the localized and possibly damaging currents in a port. Furthermore, damage in ports when facilities remain dry will be strongly related to the current speeds; a model that cannot reasonably reproduce the rotational flow patterns in a port or harbor is not likely to skillfully predict damage potential. Our analysis suggests that the local and turbulence-driven currents are an order one consideration for ports and harbors. Simply put, quantifying vertical water level rise, buoyancy forces, and straight-line current estimates are not sufficient for understanding the damage-causing hydrodynamic phenomena in ports and harbors.

While the current speeds associated with an unbounded rotational structure are significant, as an eddy approaches a solid boundary or another strong circulation, the potential for enhanced currents exists (Nicolau del Roure et al., 2009). Near moored ships, high-speed rotational flows may create unbalanced tension in mooring lines. In the

three incidents described during the 2004 Indian Ocean tsunami where the mooring lines of a large ship were broken and the ship drifted freely with the currents in the harbors (Okal et al., 2006a,b, c), each was located immediately adjacent to a 90° corner in the layout of the container terminal. It is thus put forth here that any floating or submerged object in the vicinity of such a corner in a port or harbor is significantly more likely to experience strong jet-like and rotational currents. Such considerations can and should immediately be taken into account as tsunami mitigation plans in ports and harbors are revised and updated following this most recent disaster.

Acknowledgments

The work presented here was partially supported by grants from Lighthouse R&D Enterprises Inc. and the National Science Foundation. The Port of Tauranga and Professor Willem deLange of the University of Waikato graciously provided the data used in Fig. 2.

References

- BBC, 2011. <http://www.bbc.co.uk/news/world-asia-pacific-127098562011>.
- Borrero, J.C., Cho, S., Moore, J.E., Richardson, H.W., Synolakis, C.E., 2005. Could it happen here? *Civil Eng.* 75, 455–465 133.
- Brière, C., Abadie, S., Bretel, P., Lang, P., 2007. Assessment of TELEMAC system performances, a hydrodynamic case study of Anglet, France. *Coast. Eng.* 54 (4), 345–356. doi:10.1016/j.coastaleng.2006.10.006 0378–3839.
- Dengler, L.A., Uslu, B., Barberopoulou, A., Borrero, J.C., Synolakis, C., 2008. The Vulnerability of Crescent City, California, to Tsunamis Generated by Earthquakes in the Kuril Islands Region of the Northwestern Pacific. *Seismol. Res. Lett.* 79 (5), 608–619 (September/October).
- Dengler, L., Admire, A., Uslu, B., Crawford, G., Montoya, J., Wilson, R., 2011. Observed and modeled tsunami current velocities on California's North Coast, abstract, IUGG, Melbourne July 2011.
- Gaythwaite, J., 2004. Design of marine facilities for the berthing, mooring, and repair of vessels. ASCE Publications, New York. 531 pgs.
- Griffin, W., 1984. Crescent City's dark disaster. Crescent City Printing Co., Crescent City, CA. 188 pp.

- Hinterberger, C., Frohlich, J., Rodi, W., 2007. 3D and Depth-averaged large-eddy simulations of some shallow water flows. *J. Hydraul. Eng. ASCE* 133 (8), 857–872.
- Horrillo, J., Knight, W., Kowalik, Z., 2007. The Kuril Islands tsunami of November 2006. Part II: impact at Crescent City by local amplification. *J. Geophys. Res.* VOL. ???, XXXX, DOI:10.1029.
- Jirka, 2001. Large scale flow structures and mixing processes in shallow flows. *J. Hydraul. Res.* 39 (6), 567–573.
- Kim, D.-H., Lynett, P., 2011. Turbulent mixing and scalar transport in shallow and wavy flows. *Phys. Fluids* 23 (1). doi:10.1063/1.3531716.
- Kim, D.-H., Lynett, P., Socolofsky, S., 2009. A depth-integrated model for weakly dispersive, turbulent, and rotational fluid flows. *Ocean Modell.* 27 (3–4), 198–214.
- Kowalik, Z., Horrillo, J., Knight, W., Logan, T., 2008. Kuril Islands tsunami of November 2006: 1. Impact at Crescent City by distant scattering. *J. Geophys. Res.* 113, C01020. doi:10.1029/2007JC004402 20.
- Ludwin, S., Colorado, A., 2006. "Tsunami Whirlpools – observed in 2004 and remembered in First Nations art and myth," presented at USGS Tsunami Sources Workshop <http://walrus.wr.usgs.gov/tsunami/workshop/questions.html>.
- Nicolau del Roure, F., Socolofsky, S.A., Chang, K.-A., 2009. Structure and evolution of tidal starting jet vortices at idealized barotropic inlets. *J. Geophys. Res.* 114, C05024. doi:10.1029/2008JG004997.
- Okal, E.A., Dengler, L., Araya, S., Borrero, J.C., Gomer, B., Koshimura, S., Laos, G., Olcese, D., Ortiz, M., Swensson, M., Titov, V.V., Vegas, F., 2002. A field survey of the Camaná, Peru tsunami of June 23, 2001. *Seismol. Res. Lett.* 73, 904–917.
- Okal, E.A., Fritz, H.M., Raveloson, R., Joelson, G., Pancoskova, P., Rambolamanana, G., 2006a. Madagascar field survey after the December 2004 Indian Ocean tsunami. *Earthquake Spectra* 22, S263–S283.
- Okal, E.A., Fritz, H.M., Raad, P.E., Synolakis, C.E., Al-Shijbi, Y., Al-Saifi, M., 2006b. Oman field survey after the December 2004 Indian Ocean tsunami. *Earthquake Spectra* 22, S203–S218.
- Okal, E.A., Sladen, A., Fritz, H.M., 2006c. Mauritius and Réunion Islands, field survey after the December 2004 Indian Ocean tsunami. *Earthquake Spectra* 22, S241–S261.
- Raichlen, F., 1966. Harbor resonance. In: Ippen, A.T. (Ed.), *Coastline and estuarine hydrodynamics*. McGraw-Hill, New York, NY, pp. 281–340.
- Reid, H.F., Taber, S., 1920. The Virgin Islands earthquakes of 1867–1868. *Bull. Seismol. Soc. Am.* 10, 9–30.
- Socolofsky, S.A., Jirka, G.H., 2004. Large-scale flow structures and stability in shallow flows. *J. Environ. Eng. Sci.* 3 (5), 451–462.
- Son, S., Lynett, P., Kim, D.-H., 2011. Nested and multi-physics modeling of tsunami evolution from generation to inundation. *Ocean Modell.* 38 (1–2), 96–113. doi:10.1016/j.ocemod.2011.02.007.
- Synolakis, C.E., 1995. Tsunami prediction. *Science* 270, 15–16.
- Synolakis, C.E., 2004. Tsunami and seiche. In: Chen, W.F., Scawthorn, C. (Eds.), *Earthquake Engineering Handbook*. CRC Press, pp. 9–1–9–90.
- USGS, 2011. http://earthquake.usgs.gov/earthquakes/eqinthenews/2011/usc0001xgp/finite_fault.php2011.
- Wang, X., Liu, P.L.-F., 2006. An analysis of 2004 Sumatra earthquake fault plane mechanisms and Indian Ocean tsunami. *J. Hydraul. Res.* 44 (2), 147–154.
- Wilson, R.I., Dengler, L.A., Goltz, J.D., Legg, M.R., Miller, K.M., Ritchie, A., Whitmore, P.M., 2011. Emergency response and field observation activities of geoscientists in California (USA) during the September 29, 2009, Samoa Tsunami. *Earth-Science Reviews* 107 (1–2), 193–200.